Acta Oceanol. Sin., 2024, Vol. 43, No. 4, P. 40–49
https://doi.org/10.1007/s13131-023-2253-z
http://www.aosocean.com
E-mail: ocean2@hyxb.org.cn

Thermal and exhumation history of the Songnan Low Uplift, Qiongdongnan Basin: constraints from the apatite fission-track and zircon (U-Th)/He thermochronology

Xiaoyin Tang[1, 2, 3*], Kaixun Zhang[1, 2, 3*], Shuchun Yang[4], Shuai Guo[4], Xinyan Zhao[1, 2, 3], Zhizhao Bai[4]

[1] Institute of Geomechanics, Chinese Academy of Geological Sciences, Beijing 100081, China

[2] Key Laboratory of Paleomagnetism and Tectonic Reconstruction, Ministry of Natural Resources, Beijing 100081, China

[3] Key Laboratory of Petroleum Geomechanics, China Geological Survey, Beijing 100081, China

[4] China National Offshore Oil Corporation (CNOOC) Research Center, Beijing 100028, China

Received 4 July 2023; accepted 12 September 2023

© Chinese Society for Oceanography and Springer-Verlag GmbH Germany, part of Springer Nature 2024

Abstract

Significant advancements have been made in the study of Mesozoic granite buried hills in the Songnan Low Uplift (SNLU) of the Qiongdongnan Basin. These findings indicate that the bedrock buried hills in this basin hold great potential for exploration. Borehole samples taken from the granite buried hills in the SNLU were analyzed using apatite fission track (AFT) and zircon (U-Th)/He data to unravel the thermal history of the basement rock. This information is crucial for understanding the processes of exhumation and alteration that occurred after its formation. Thermal modeling of a sample from the western bulge of the SNLU revealed a prolonged cooling event from the late Mesozoic to the Oligocene period (~80–23.8 Ma), followed by a heating stage from the Miocene epoch until the present (~23.8 Ma to present). In contrast, the sample from the eastern bulge experienced a more complex thermal history. It underwent two cooling stages during the late Mesozoic to late Eocene period (~80–36.4 Ma) and the late Oligocene period (~30–23.8 Ma), interspersed with two heating phases during the late Eocene to early Oligocene period (~36.4–30 Ma) and the Miocene epoch to recent times (~23.8–0 Ma), respectively. The differences in exhumation histories between the western and eastern bulges during the late Eocene to Oligocene period in the SNLU can likely be attributed to differences in fault activity. Unlike typical passive continental margin basins, the SNLU has experienced accelerated subsidence after the rifting phase, which began around 5.2 Ma ago. The possible mechanism for this abnormal post-rifting subsidence may be the decay or movement of the deep thermal source and the rapid cooling of the asthenosphere. Long-term and multi-episodic cooling and exhumation processes play a key role in the alteration of bedrock and contribute to the formation of reservoirs. On the other hand, rapid post-rifting subsidence (sedimentation) promotes the formation of cap rocks.

Key words: granite buried hills, (U-Th)/He dating, fission-track dating, exhumation, Songnan Low Uplift

Citation: Tang Xiaoyin, Zhang Kaixun, Yang Shuchun, Guo Shuai, Zhao Xinyan, Bai Zhizhao. 2024. Thermal and exhumation history of the Songnan Low Uplift, Qiongdongnan Basin: constraints from the apatite fission-track and zircon (U-Th)/He thermochronology. Acta Oceanologica Sinica, 43(4): 40–49, doi: 10.1007/s13131-023-2253-z

1 Introduction

Granite buried hill oil and gas reservoirs have emerged as a novel area of interest in the field of oil and gas exploration. Notable discoveries of large granite bedrock oil and gas fields have been made in various countries such as Vietnam, Libya, Venezuela, and India (Pan et al., 2007), thereby opening up new avenues for exploration in buried hill formations. Consequently, geologists both domestically and internationally have increasingly focused their attention on bedrock oil and gas reservoirs (Ma et al., 2006). Notably, significant progress has been made in the exploration of buried-hill oil and gas reservoirs in Chinese waters, particularly in the Bohai Sea region (Deng, 2015; Hu et al., 2020; Xu et al., 2019a). In recent years, the drilling of high-quality gas reservoirs has been successful in the deltaic sandstone and granitic basement buried hill within the Y8-1 structure of the Songnan Low Uplift (SNLU) in the Qiongdongnan Basin (QDNB). Subsequently, thick and high-quality gas reservoirs with substantial gas flow rates have been discovered in the Mesozoic basement of the Y8-3 structure (Shi et al., 2019; Zhang et al., 2019). These findings indicate promising prospects for exploration in the basement burial-hill area of the SNLU and mark the beginning of a new era in natural gas exploration in the northern South China Sea (SCS).

The formation of large oil and gas fields is heavily dependent on favorable reservoir conditions. In the case of granite, which is inherently compact, it requires subsequent modifications to become an effective reservoir. Therefore, it is crucial to comprehend the evolutionary process of buried granite hills following

Foundation item: The National Natural Science Foundation of China under contract No. 42072181; the CNOOC Research Project "Resource Potential, Reservoir Formation Mechanism and Breakthrough Direction of Potential Oil-rich Depressions in Offshore Basins of China (YXKY-ZX 01 2021)".

*Corresponding author, E-mail: xytang2019@126.com; zhangkaixun@126.com

their formation. Previous research suggests that the buried hills in the SNLU were formed during the Mesozoic era (Mi et al., 2023) and have undergone long-term uplift, weathering, and denudation (Tang et al., 2017; Xu et al., 2019b). However, due to limited data availability, the specific details regarding their post-formation uplift and exhumation history remain unclear, impeding our understanding of the exhumation weathering process of these buried hills.

Low-temperature thermochronological methods, such as zircon and apatite fission track (AFT) and (U-Th)/He dating, have proven to be effective tools for constraining shallow crustal processes (Chang et al., 2017, 2018; Ehlers and Farley, 2003; Gallagher et al., 1998; Qiu et al., 2010, 2014; Sehrt et al., 2017; Stockli, 2005; Tu et al., 2021). In this study, we present, for the first time, zircon (U-Th)/He and apatite fission track data of the basement granite in different tectonic units of the SNLU. Based on these data, we decipher the thermal and exhumation processes of the buried hills during the late Mesozoic-Cenozoic period and further discuss the underlying genetic mechanism. This research is significant as it enhances our understanding of the development period and modification conditions of the buried hill reservoir in the study area, providing valuable geological theory support for future exploration endeavors.

2 Geologic setting

The SCS is a large marginal basin in the western Pacific region that formed in a complex tectonic setting influenced by the Pacific, Indo-Australian, and Eurasian plates (Cullen et al., 2010). The initial rifting in the SCS likely began in the late Cretaceous to early Paleocene, when the stress field changed from compression to extension (Clift and Lin, 2001; Franke et al., 2014). Following multiple phases of rifting (Clift and Lin, 2001; Ru and Pigott, 1986), the continent broke apart and the SCS basin started to open (Briais et al., 1993; Li et al., 2014). The exact timing of seafloor spreading in the SCS is still debated, but it is generally believed to have started around 33 Ma ago and ended around 15.5 Ma ago (Li et al., 2014, 2015). Along the northern margin of the SCS, several sedimentary basins formed, including the Pearl River Mouth Basin (PRMB) and the QDNB (Fig. 1a).

The QDNB, located on the northwestern continental margin

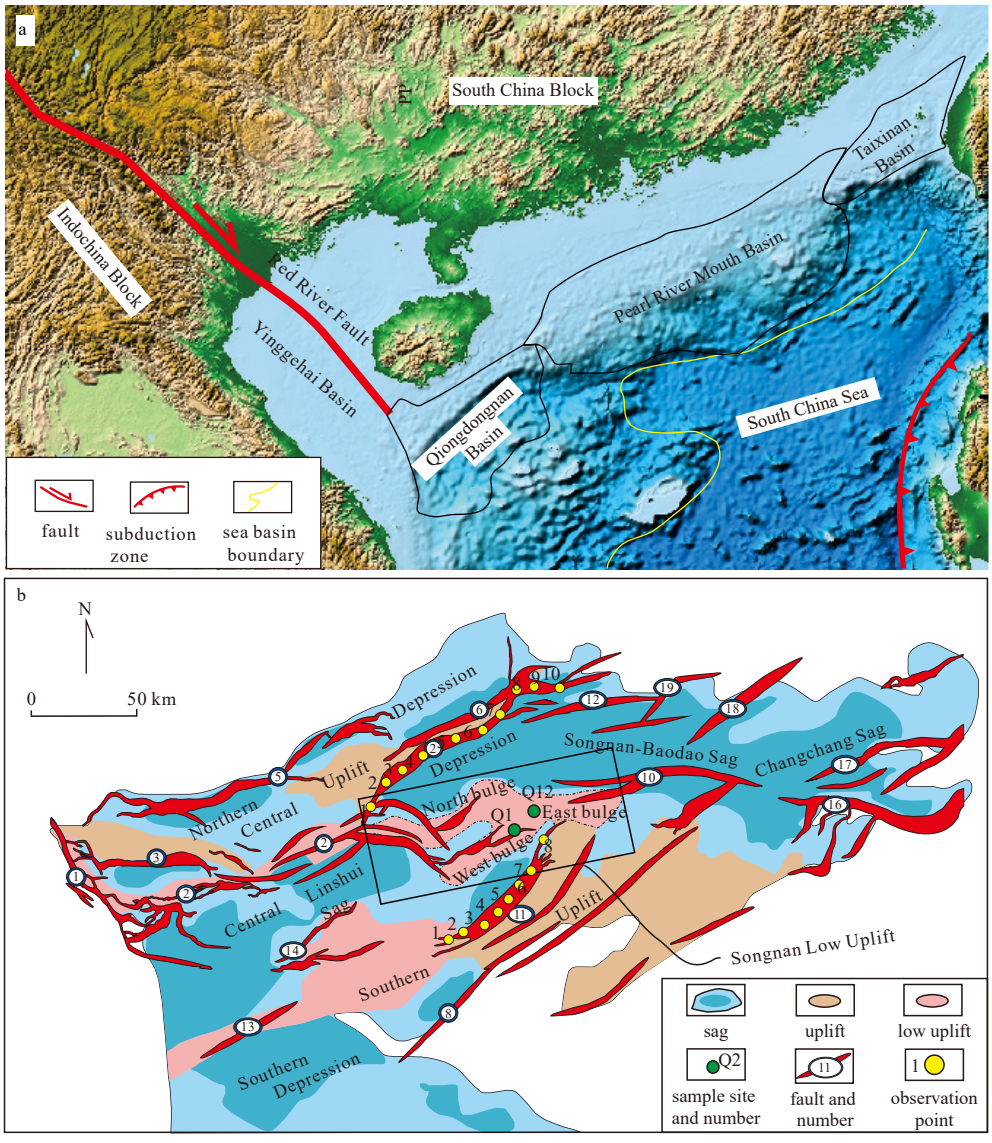

Fig. 1. Regional geological outline of the Qiongdongnan Basin (QDNB) (a), and the basin tectonic units (b). Fault distribution and observation points in b are from Zhou et al. (2019).

of the SCS, is a rift basin that developed on the Pre-Cenozoic basement. It is bounded by Hainan Island to the north, the Yinggehai Basin to the west, and the PRMB to the east (Fig. 1a). The basin can be divided into five tectonic belts from north to south: the Northern Depression, Central Uplift, Central Depression, Southern Uplift, and Southern Depression (Fig. 1b). Throughout the Cenozoic era, the basin underwent three stages: syn-rifting, post-rifting thermal subsidence, and post-rifting accelerated subsidence (Fig. 2) (Clift and Sun, 2006; Ren et al., 2014; Shi et al., 2017; Zhao et al., 2013). Sequence stratigraphy has been established based on seismic horizons and drilling well data, including the Lingtou Formation (Eocene), Yacheng Formation (lower Oligocene), Lingshui Formation (upper Oligocene), Sanya Formation (lower Miocene), Meishan Formation (middle Miocene), Huangliu Formation (upper Miocene), Yinggehai Formation (Pliocene), and Ledong Formation (Quaternary) (Cheng et al., 2021) (Fig. 2).

The study area, known as the SNLU, is located in the Central Depression of the QDNB, adjacent to the Lingshui Sag, Songnan-Baodao Sag, and Changchang Sag. The low uplift, which generally trends in the east-west direction, has been affected by secondary faults and can be further divided into the north bulge, west bulge, and east bulge (see Fig. 1b). In the study area, the Eocene Lingtou Formation is generally absent, and the Yacheng and Lingshui Formations are partially missing (Zhou et al., 2019).

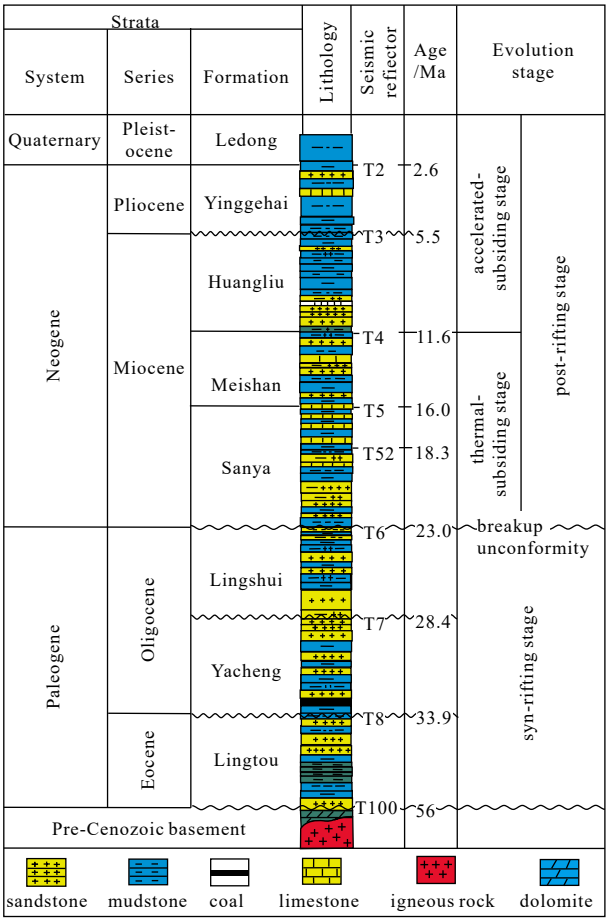

Fig. 2. Comprehensive stratigraphic column of the Qiongdongnan Basin modified from Ji et al. (2021), Ren et al. (2022), and Wang et al. (2015).

3 Sample description

Two cutting samples were collected from the hydrocarbon exploration boreholes Q1 and Q12, which were drilled by the China National Offshore Oil Company. Borehole Q1 was situated on the western protrusion, while Borehole Q12 was situated on the eastern protrusion of the SNLU (refer to Fig. 1 for locations and Table 1 for sample details).

The major and trace element compositions of the two samples have been previously reported by Mi et al. (2023). Sample Q1 exhibit contents of SiO_2 (63.43 wt%), Al_2O_3 (12.67 wt%), MgO (0.47 wt%), Fe_2O_3 (1.82 wt%), and CaO (13.06 wt%). Sample Q12 exhibit contents of SiO_2 (64.56 wt%), Al_2O_3 (15.39 wt%), MgO (1.38 wt%), Fe_2O_3 (4.92 wt%), and CaO (4.76 wt%). These compositions place both samples within the quartz monzonite fields in the Total alkali silica classification diagram (Fig. 3a) and classify them as the high K calc-alkaline series (Fig. 3b). The plot of Ga/Al vs. Ce categorizes the samples into the I- and S-type field (Fig. 3c). Furthermore, the A/NK versus A/CNK plot (Fig. 3d) and the Rb versus Th plot (Fig. 3e) confirm their classification as I-type samples.

Normalized to chondrite, the quartz monzonites in this study show enrichment of light rare earth elements (LREE) and negative anomalies of Eu (Fig. 4a). When normalized to the primitive mantle, the samples exhibit positive anomalies in K and Pb, and negative anomalies in Nb, Ta, P, Zr, and Ti, (Fig. 4b). The Rb vs. Y + Nb plot (Fig. 3f) indicates that the samples fall into the volcanic arc field, as described by Pearce et al. (1984). Additionally, the rocks exhibit well-defined negative anomalies of Ta, Nb, and Ti (Fig. 4b), presenting the characteristics of subduction-related magmas, as defined by Sajona et al. (1993). In conclusion, the samples in this study display characteristics consistent with I-type affinity and were likely formed in a volcanic arc environment, possibly associated with the subduction of the Paleo-Pacific plate (Mi et al., 2023).

4 Analytical methods

Zircon and apatite grains separation were performed at the Chengxin Geological Services Co. LTD, in Langfang, Hebei Province, China, following the standard heavy mineral separation techniques.

4.1 *Apatite fission track*

Apatite fission track (AFT) analysis was conducted at the State Key Laboratory of Earthquake Dynamics, Institute of Geology, China Earthquake Administration. Apatite fission track ages were obtained using the LA-ICP-MS method and calculated by the zeta calibration method (Hasebe et al., 2004; Pang et al., 2017). NIST612 was used as an external standard to measure the signal intensity and Durango apatite (31.4 Ma ± 0.5 Ma) was chosen as the age-calibration standard. Spontaneous fission tracks were etched in 5.5 N HNO_3 at 21℃ for 20 s.

χ^2 test was performed to assess the homogeneity of AFT ages. When $P(\chi^2) > 5\%$, the single-grain AFT ages are assumed to be-

Table 1. Sample information

Sample	U-Pb age/Ma	Burial temperature/℃	Lithology	Overlying strata
Q1	228.9 ± 1.0	~ 63	quartaz monzonite	Sanya Formation
Q12	270.0 ± 1.2	~ 75	quartaz monzonite	Yacheng Formation

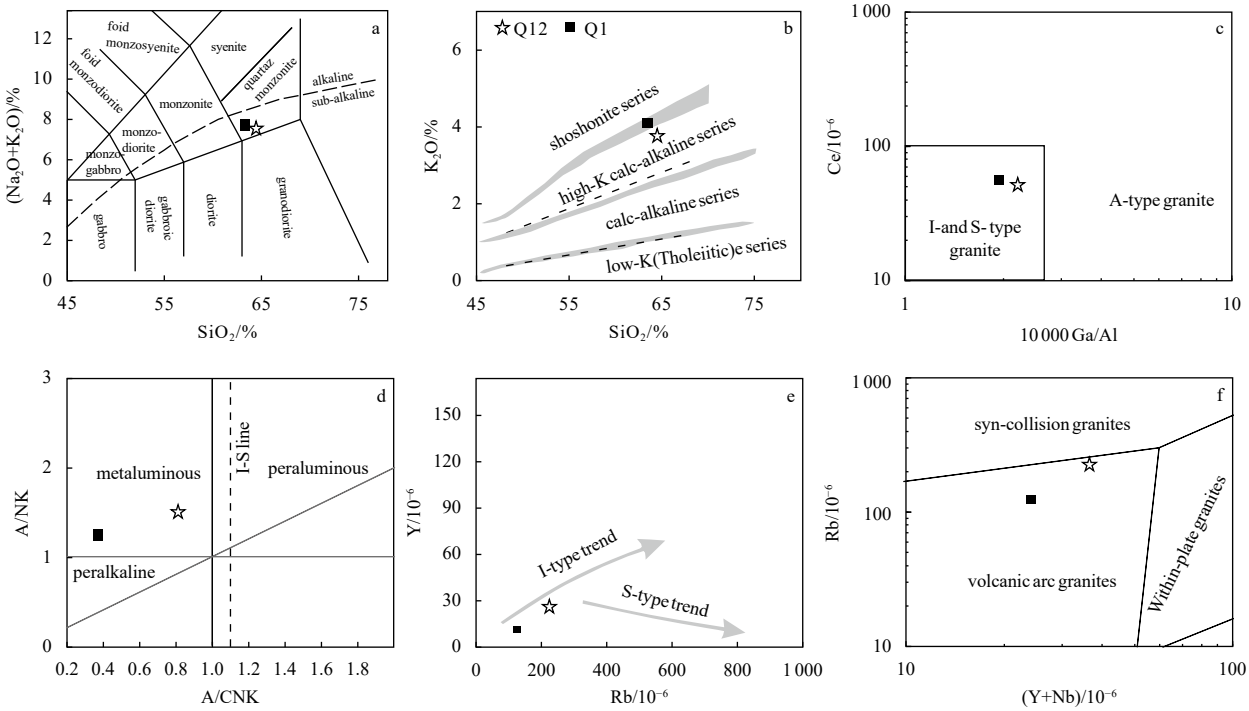

Fig. 3. Sample geochemical features. a. SiO_2 vs. K_2O+Na_2O (Middlemost, 1994); b. SiO_2 vs. K_2O scheme (Rickwood, 1989); c. 10 000 Ga/Al vs. Ce plot (Whalen et al., 1987); d. A/CNK vs. A/NK diagram (Maniar and Piccoli, 1989); e. Rb vs. Y plot (Chappell, 1999); and f. (Y+Nb) vs. Rb plot (Pearce et al., 1984).

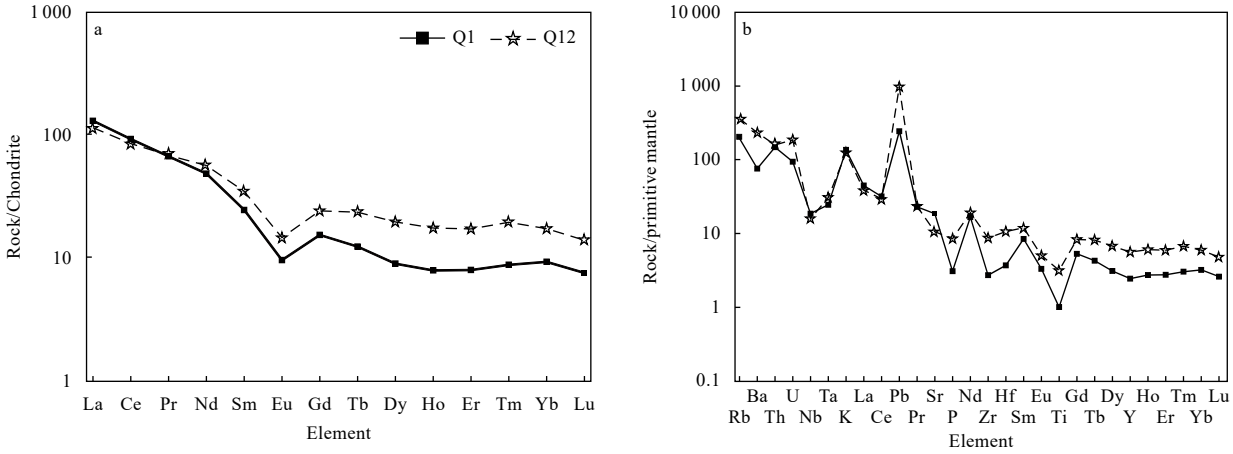

Fig. 4. Chondrite-normalized REE patterns (a) and primitive mantle normalized trace element patterns (b) of the basement samples.

long to the same age population and relate to the same thermal event, then the central age is adopted as the AFT age of the sample. Otherwise, a $P(\chi^2)$ of < 5% indicates a heterogeneous age distribution, with the resulting age being mixed.

4.2 *Zircon (U-Th)/He*

For zircon (U-Th)/He (ZHe) dating, zircon grains were picked after the recommendations of Farley (2002). Single zircon grains were loaded into Nb micro-tubes, then in-vacuum degassed by laser at ~1 250℃ and analyzed for ^{4}He by isotope dilution on noble-gas mass-spectrometer using the Helium extraction line in the State Key Laboratory of Earthquake Dynamics, Institute of Geology, China Earthquake Administration. Degassed zircon was dissolved and analyzed for U and Th on ICP-MS according to the procedures of Evans et al. (2005). Standard α-ejection correction and volume estimates were made using measured grain dimensions and assuming an orthorhombic prism geometry with pyramid terminations according to Ketcham et al. (2011). More details in method information can be found in Li et al. (2017).

5 Results

5.1 *AFT results*

The AFT dating results are shown in Table 2 and Fig. 5. All the samples pass the χ^2 test, demonstrating that all the single-grain ages form a single population. Sample Q1 yielded a central age of 69.2 Ma ± 2.6 Ma. Confined track length distributions are unimodal with the MTL (mean confined track length) of (12.26 ± 0.28) μm. Sample Q12 presented a central age of 60.1 Ma ± 3.4 Ma. The confined track length distribution is unimodal with the MTL of 11.79 μm and a standard deviation of 1.26 μm. The short MTL values imply the thermal annealing of fission tracks.

Table 2. Apatite fission-track data

Sample	N_c	N_s	ρ_s /(10^5cm^{-2})	^{238}U /10^{-6}	$P(\chi 2)$/%	Central age (Ma ± 1σ)	N_L	MTL (μm ± 1σ)	SD	D_{par} (μm ± SD)
Q1	32	825	2.427	7.22	68	69.2 ± 2.6	24	12.26 ± 0.28	1.39	1.71 ± 0.23
Q12	33	367	3.22	10.49	64	60.1 ± 3.4	18	11.79 ± 0.29	1.26	1.51 ± 0.13

N_c: number of apatite crystals analyzed; N_s: total number of fission tracks counted; ρ_s: spontaneous track density; $P(\chi^2)$: chi-square probability that all single-crystal ages represent a single population of ages where degrees of freedom = N_{c-1}; N_L: number of confined track lengths measured: MTL: Mean confined track length; SD: standard deviation; D_{par}: mean track etch pit diameter parallel to the crystallographic c-axis; Apatite-Zeta NIST610 = 1 940 ± 50.

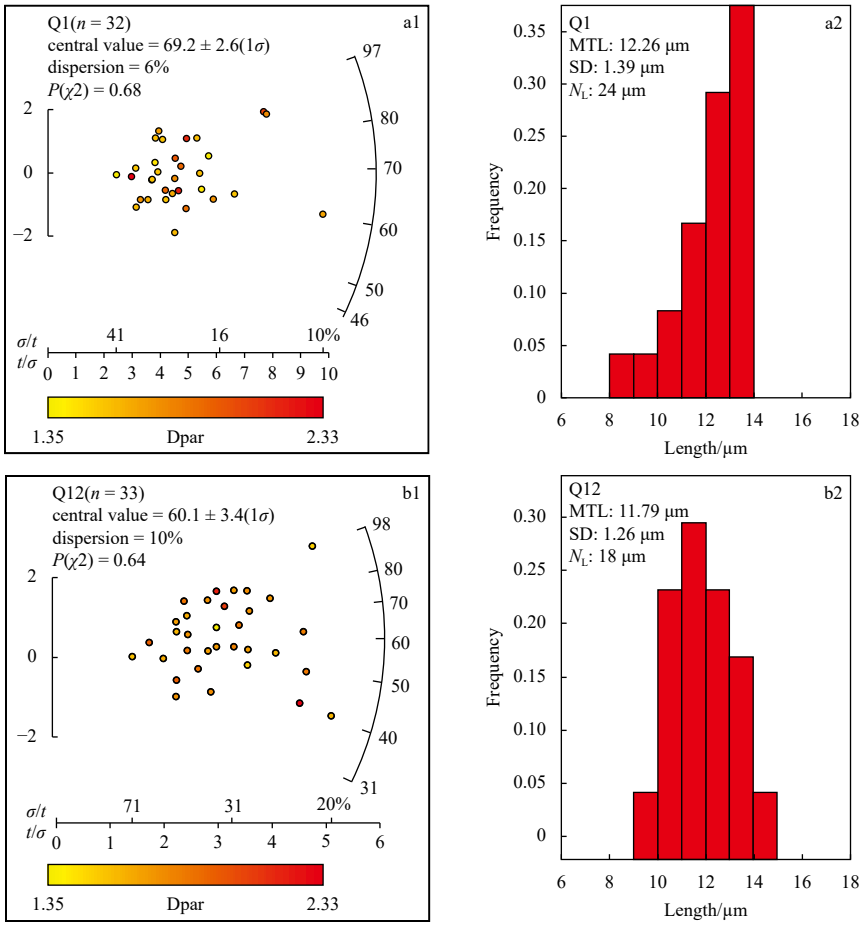

Fig. 5. Radial plots of apatite fission-track (left) and confined track length histograms (right). Central ages are calculated using RadialPlotter (Vermeesch, 2009). MTL-mean track length, SD-standard deviation, N_L-number of spontaneous tracks.

5.2 *ZHe results*

Seven single grains from the two samples were analyzed by ZHe dating (Table 3). Three zircon grains from Sample Q1 yielded ZHe ages of 486.1 Ma ± 11.6 Ma (Q1-1), 248.5 Ma ± 5.8 Ma (Q1-2), and 103.7 Ma ± 6.5 Ma (Q1-3). Q1-1 and Q1-2 were excluded because the ZHe ages were older than the granitoid emplacement age (228.9 Ma ± 1.0 Ma) (Mi et al., 2023). Q1-3 was not considered in the following thermal history modeling because single grain ZHe age is not convincing. For Sample Q12, excluding the outlier of 152.7 Ma ± 2.64 Ma (Q12-4), other three zircon grains from the sample yielded ZHe ages of 45.3 Ma ± 1.0 Ma to 73.9 Ma ± 1.3 Ma, with a mean of 61.4 Ma ± 1.3 Ma.

Table 3. Zircon (U-Th)/He data

Sample	^{238}U /10^{-6}	±1σ /10^{-6}	^{232}Th /10^{-6}	±1σ/10^{-6}	He (ncc)	±1σ /ncc	Unc. age/Ma	±1σ/Ma	R_s/μm	F_T	Cor. age/Ma	±1σ/Ma
Q1-1	100.5	2.4	41.7	1.0	21.454 1	0.258 5	368.5	8.8	46.7	0.758	486.1	11.6
Q1-2	97.7	2.3	34.0	0.9	16.197 5	0.160 5	205.1	4.8	51.5	0.825	248.5	5.8
Q1-3	222.4	5.0	56.0	1.2	22.400 5	0.221 5	83.4	1.9	57.4	0.804	103.7	2.4
Q12-1	2 013.2	44.6	490.6	11.2	26.036 3	0.280 8	47.2	1.1	40.7	0.727	65.0	1.5
Q12-2	1 711.5	36.5	487.5	12.3	12.010 9	0.132 8	31.2	0.7	34.5	0.689	45.3	1.0
Q12-3	715.1	11.5	174.3	2.3	12.912 5	0.130 8	57.3	1.0	38.5	0.775	73.9	1.3
Q12-4	334.17	5.02	79.89	0.96	11.347 8	0.114 9	116.3	2.01	37.0	0.762	152.7	2.64

R_s: sphere equivalent radius of hexagonal crystal; F_T: alpha ejection correction factor.

6 Thermal history reconstruction

6.1 *Modeling approach*

HeFty (Ketcham et al., 2018) was used to further investigate the thermal evolution of basement samples of the SNLU. ZHe data were modeled using the He diffusion kinetic parameters from Guenthner et al. (2013). Alpha-particle stopping distances and α-ejection age corrections were conducted after the method in Ketcham et al. (2011). Apatite fission track ages and projected fission track lengths with Dpar as a kinetic parameter are included in the annealing model of Ketcham et al. (2007).

We follow a model strategy that was described in Tang et al. (2019). Besides the AFT and ZHe results achieved in this work, the following border conditions for the modeling were also assumed: (1) initial early constraint, placed above Tc of highest-T system or population modeled, at least 1.5 times of the oldest age; (2) the paleo-surface temperature when the samples deposited assumed to be (15 ± 10)℃; and (3) the present-day burial temperature.

6.2 *Modeling results*

All modeled paths presented in Fig. 6 resulted in high goodness of fit (GOF > 0.86) between the measured input data and modeled output data.

Although the two samples are located next to each other, they have experienced different thermal histories (Fig. 6). Sample Q1 from the western bulge of the SNLU shows an overall pattern with a two-phase thermal history: (1) a protracted cooling from the late Cretaceous to the early Miocene, and (2) a subsequent heating stage until the recent times (Fig. 6a1). Comparatively, Sample Q12 from the eastern bulge of the SNLU has undergone a more complex thermal evolution, with an overall pattern of four stages: (1) a major late Cretaceous-late Eocene cooling, (2) heating during the period of late Eocene-early Oligocene, (3) a minor cooling in the late Oligocene, and (4) a reheating from the early Miocene till present (Fig. 6b1).

7 Discussions

Constrained by the AFT and ZHe data, thermal history modeling results, as the weighted mean t-T paths presented in Fig. 7, indicate that samples from the western and eastern bulge of the SNLU have experienced differential cooling and corresponding exhumation during the late Eocene to Oligocene, followed by heating from the early Miocene to recent times, which was characterized with a rapid heating phase since the early Pliocene.

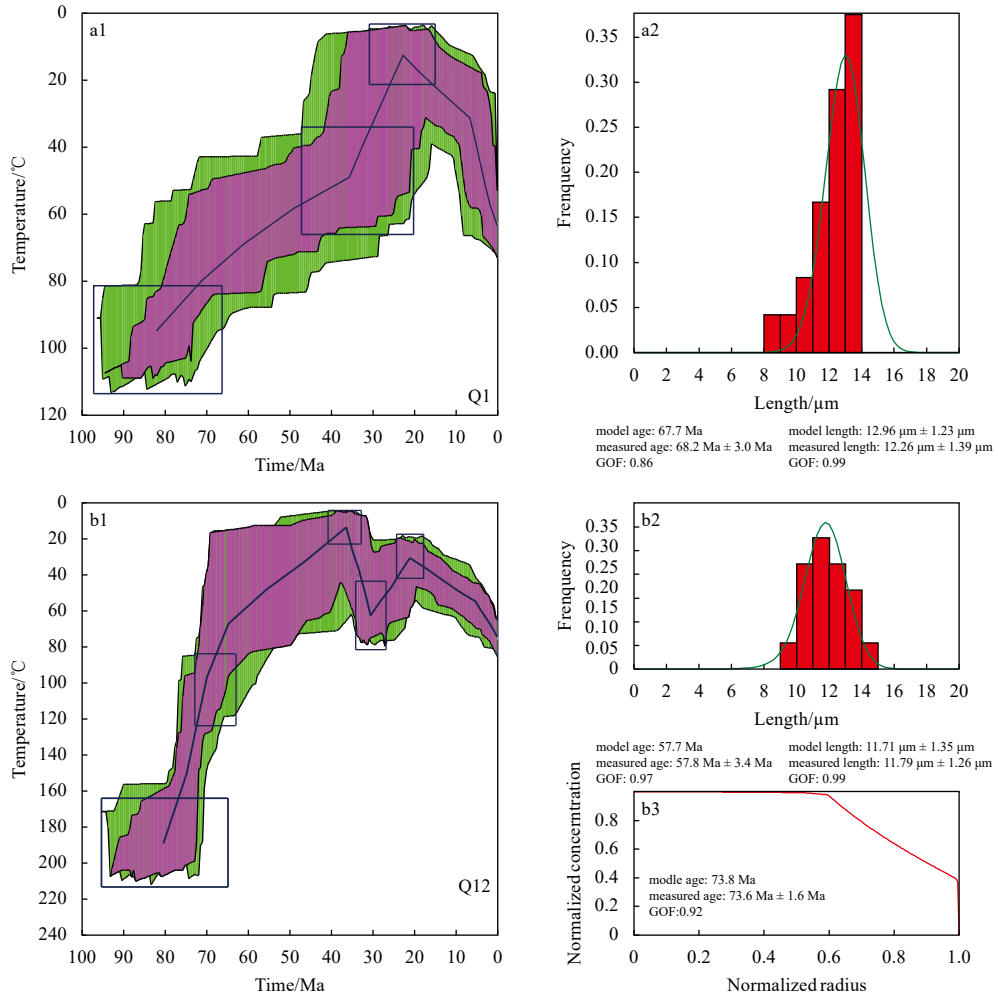

Fig. 6. Modeling results for Sample Q1 (a) from the western bulge of the Songnan Low Uplift and Sample Q12 (b) from the eastern bulge. Illustrated are the t-T paths on the left (a1 and b1) with the corresponding confined fission-track length frequency distribution (a2 and b2) and the ZHe diffusion profile (b3) on the right. The t-T paths on the left show different fits: green paths, acceptable fit (GOF ⩾ 5%); pink paths, good fit (GOF ⩾ 50%); black line, weighted mean path.

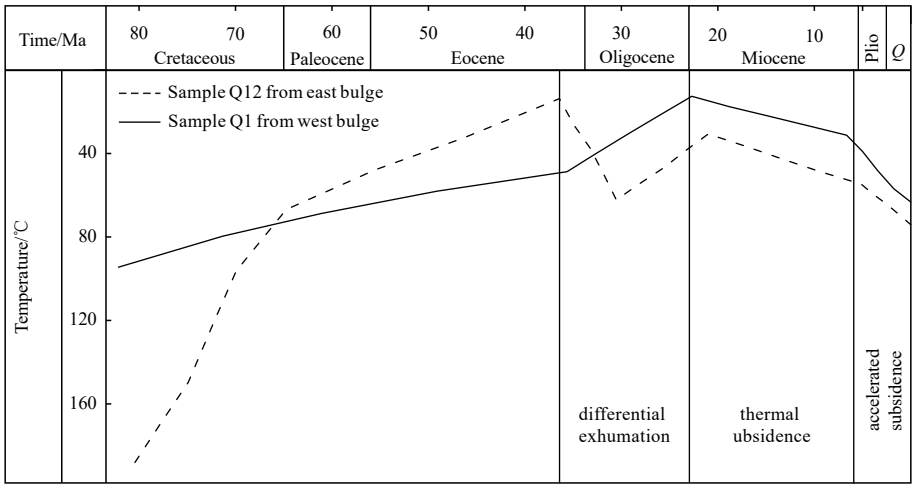

Fig. 7. Comparative presentation of weighted mean paths from thermal models. The dashed line is the weighted mean thermal history for Sample Q12 from the east bulge, and the solid line is the weighted mean thermal history for Sample Q1 from the west bulge.

7.1 *Origin of the differential exhumation on the west and east bulge of the Songnan Low Uplift*

Fault activity plays a crucial role in the formation and evolution of basins (Xie et al., 2007). In the QDNB, basement faults are predominantly oriented in the NE-SW direction (Fig. 1). Among these faults, No.2 and No.11 are the primary controlling factors influencing the tectonic evolution of the SNLU (Zhou et al., 2019). During the late Eocene to early Oligocene, the No.11 fault exhibited higher activity intensity compared to the No.2 fault (Fig. 8). Spatially, the No.11 fault displayed stronger activity in the west and weaker activity in the east (Fig. 8b), resulting in a corresponding high-to-low gradient in the SNLU with an overall eastward dip. On the other hand, the No.2 fault exhibited clear segmentation and can be divided into the Songnan section and Baodao section, both with similar activity rates (Fig. 8a) (Zhou et al., 2019). Consequently, while the western bulge experienced uplift and denudation (cooling) between approximately 36 Ma and 30 Ma, the eastern bulge underwent heating due to sedimentation of the Yacheng Formation.

During the late Oligocene, the activity intensity of the middle part of the No.2 fault significantly increased, reaching up to 550 m/Ma (Fig. 8a). As a result, the eastern bulge, located on the hanging wall of the No.2 fault, became warped and uplifted. Meanwhile, the No.11 fault entered an inheriting activity stage, with the activity center gradually shifting eastward (Fig. 8b). Consequently, the western bulge continued to uplift, and the activity of the No.11 fault influenced the eastern bulge, accelerating its uplift (Zhou et al., 2019). Consequently, both the western and eastern bulges of the SNLU experienced cooling and exhumation between approximately 30 Ma and 23.8 Ma (Fig. 7). In summary, differential fault activities resulted in the differential exhumation of the western and eastern bulges of the SNLU during the late Eocene to Oligocene.

7.2 *Post-rifting accelerated subsidence and its origin*

During the early Miocene, the process of rifting weakened and large-scale faulting ceased. Subsequently, the QDN (name of the region) entered a post-rifting stage (Xie et al., 2007; Zhao et al., 2013). Based on the modeled temperature-time (t-T) paths, the temperature gradually increased from approximately 12.6–30.8℃ to a range of 31.3–54.9℃ between ~ 22–5.2 Ma. From around 5.2 Ma onwards, the temperature rapidly increased to its present state (Fig. 6). This rapid heating is commonly attributed to enhanced sedimentation caused by accelerated subsidence during the post-rifting stage. This is supported by the simultaneous occurrence of rapid sedimentation (Cheng et al., 2021; Zhao et al., 2013, 2015) and anomalous subsidence in the QDNB region, as observed in previous studies (Li et al., 2012; Mao et al.,

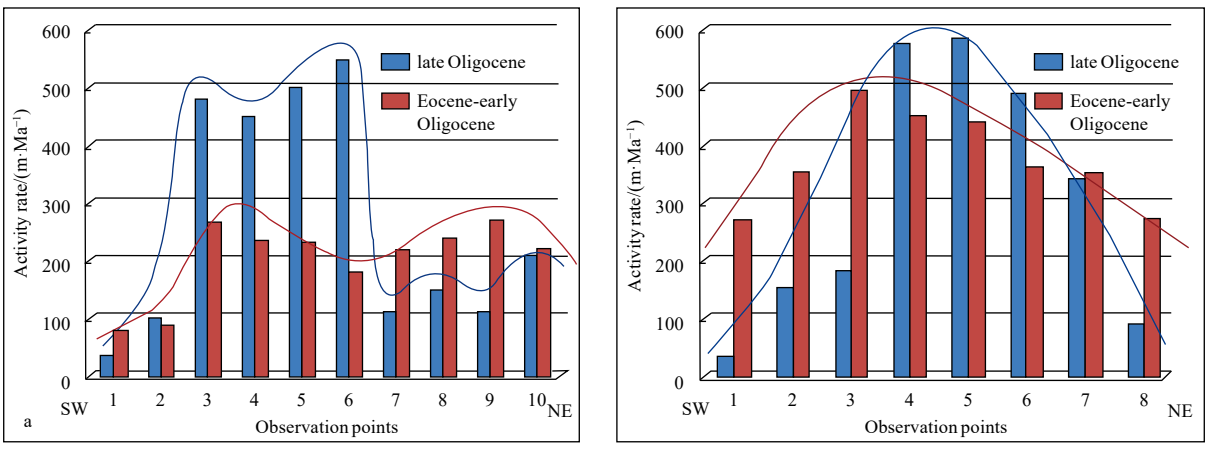

Fig. 8. Activity rate of the main controlling faults in the Songnan Low Uplift during the Eocene-early Oligocene and late Oligocene. a. No.2 fault, b. No.11 fault (Zhou et al., 2019). For locations of the observation points see Fig. 1b.

2015; Shi et al., 2017; Xie et al., 2006; Yuan et al., 2008; Zhao et al., 2018; 2013). Assuming a geothermal gradient of 31.9℃/km (Yuan et al., 2009), the thermal models suggest a subsidence rate of approximately 37–47 m/Ma during the thermal subsiding stage, but as high as 119–152 m/Ma during the accelerated subsiding stage. These subsidence rates align with values obtained through seismic interpretation (Zhao et al., 2013).

The observed features in the QDNB region deviate from the expected exponential decay pattern of thermal subsidence after rifting, as observed in the typical Atlantic passive margin (McKenzie, 1978; Steckler and Watts, 1978). While the phenomenon is well-established and widely accepted, the underlying tectonic mechanism remains a subject of debate. Several hypotheses have been proposed to explain the rapid subsidence observed in the QDNB region following rifting. These include the possibility of a new rifting episode and polarity change of the Red River fault (Yuan et al., 2008), dynamic topography (Xie et al., 2006), and lower crustal flow (Lei et al., 2013; Zhao et al., 2013).

It has been suggested that further crustal thinning resulting from a new rifting episode could lead to rapid post-rifting subsidence. However, faulting analyses indicate that there has been minimal faulting since the late Miocene (Zhao et al., 2013), making a new rifting episode unlikely. Another proposal suggests that the dextral strike-slip motion of the Red River fault in the late Miocene could be responsible for the rapid post-rifting subsidence (Yuan et al., 2008). While this fault motion may explain the rapid subsidence observed in the western QDNB region, it fails to account for the larger magnitude of subsidence observed in the eastern QDNB region (Shi et al., 2017; Yang et al., 2015). In theory, dynamic topography is a possible mechanism to cause abnormal post-rifting subsidence. However, the calculation of the dynamic topography model involves numerous uncertain parameters, leading to controversy regarding the predicted amount of abnormal subsidence (Xie et al., 2006). The lower crustal flow model, as suggested by Morley and Westaway (2006), contradicts gravitational buoyancy forces and is deemed unlikely to be valid (Allen et al., 2004). This model posits that lower crustal material would flow from the basin area (low pressure) to the sediment source area (high pressure). However, the uniformity in the whole crust stretch, as indicated by the thinning factors of the entire crust and the upper crust, suggests that lower crustal flow is improbable (Shi et al., 2017; Yang et al., 2015).

It is important to note that all the aforementioned hypotheses solely focus on the mechanism associated with the rapid post-rifting subsidence episode. However, observations in the QDNB reveal not only additional post-rifting thermal subsidence but also a deficit in syn-rifting tectonic subsidence (Shi et al., 2017). Therefore, we favor the mechanism proposed by Shi et al. (2017), which suggests that the rapid post-rifting subsidence may be linked to the decay of a deep thermal anomaly and the swift cooling of the asthenosphere. Evidence of the deep thermal anomaly is supported by magmatic intrusions identified through drilling and seismic data in the QDNB (Lu et al., 2011; Tang et al., 2013), as well as the presence of continuous low-velocity bodies beneath the adjacent areas of Hainan Island, as revealed by tomography (Lei et al., 2009).

8 Conclusions

This study presents the first dataset of AFT and ZHe thermochronology for the SNLU in the QDNB, located in the northern SCS. The findings of this study can be summarized as follows:

(1) The granite buried hills in the SNLU underwent long-term cooling and subsequent uplift after their formation. However, differential exhumation occurred in the western and eastern bulges during the late Eocene to Oligocene period.

(2) During the late Eocene to early Oligocene, the west bulge experienced uplift and denudation, while the east bulge was subjected to deposition and burial. Subsequently, both the west and east bulges uplifted and eroded together during the Late Oligocene. The differential exhumation evolution was primarily influenced by the varying activity of faults.

(3) In contrast to typical passive continental margin basins, both the west and east bulges underwent an accelerated post-rifting subsidence stage from approximately 5.2 Ma ago to the present. This phenomenon is likely attributed to the decay of a deep thermal anomaly and rapid cooling of the asthenosphere.

Acknowledgements

We are grateful to Jianzhang Pang and Ying Wang for their help during the analyses of the samples. We give our sincerest thanks to three anonymous reviewers for their constructive comments that improved the manuscript greatly.

References

Allen M, Jackson J, Walker R. 2004. Reply to comment by Rob Westaway on “Late Cenozoic reorganization of the Arabia-Eurasia collision and the comparison of short-term and long-term deformation rates”. Tectonics, 23(5): TC5007

Briais A, Patriat P, Tapponnier P. 1993. Updated interpretation of magnetic anomalies and seafloor spreading stages in the South China Sea: implications for the Tertiary tectonics of Southeast Asia. Journal of Geophysical Research: Solid Earth, 98(B4): 6299–6328, doi: 10.1029/92JB02280

Chang Jian, Qiu Nansheng, Zhao Xianzheng, et al. 2018. Mesozoic and Cenozoic tectono-thermal reconstruction of the western Bohai Bay Basin (East China) with implications for hydrocarbon generation and migration. Journal of Asian Earth Sciences, 160: 380–395, doi: 10.1016/j.jseaes.2017.09.008

Chang Jian, Tian Yuntao, Qiu Nansheng. 2017. Mid-Late Miocene deformation of the northern Kuqa fold-and-thrust belt (southern Chinese Tian Shan): An apatite (U-Th-Sm)/He study. Tectonophysics, 694: 101–113, doi: 10.1016/j.tecto.2016.12.003

Chappell B W. 1999. Aluminium saturation in I- and S-type granites and the characterization of fractionated haplogranites. Lithos, 46(3): 535–551, doi: 10.1016/S0024-4937(98)00086-3

Cheng Cong, Jiang Tao, Kuang Zenggui, et al. 2021. Seismic characteristics and distributions of Quaternary mass transport deposits in the Qiongdongnan Basin, northern South China Sea. Marine and Petroleum Geology, 129: 105118, doi: 10.1016/j.marpetgeo.2021.105118

Clift P, Lin Jian. 2001. Preferential mantle lithospheric extension under the South China margin. Marine and Petroleum Geology, 18(8): 929–945, doi: 10.1016/S0264-8172(01)00037-X

Clift P D, Sun Zhen. 2006. The sedimentary and tectonic evolution of the Yinggehai–Song Hong basin and the southern Hainan margin, South China Sea: Implications for Tibetan uplift and monsoon intensification. Journal of Geophysical Research: Solid Earth, 111(B6): B06405

Cullen A, Reemst P, Henstra G, et al. 2010. Rifting of the South China Sea: new perspectives. Petroleum Geoscience, 16(3): 273–282, doi: 10.1144/1354-079309-908

Deng Yunhua. 2015. Formation mechanism and exploration practice of large-medium buried-hill oil fields in Bohai Sea. Acta Petrolei Sinica (in Chinese), 36(3): 253–261

Ehlers T A, Farley K A. 2003. Apatite (U-Th)/He thermochronometry: methods and applications to problems in tectonic and surface processes. Earth and Planetary Science Letters, 206(1–2): 1–14, doi: 10.1016/S0012-821X(02)01069-5

Evans N J, Byrne J P, Keegan J T, et al. 2005. Determination of uranium and thorium in zircon, apatite, and fluorite: Application to laser (U-Th)/He thermochronology. Journal of Analytical

Chemistry, 60(12): 1159–1165, doi: 10.1007/s10809-005-0260-1
Farley K A. 2002. (U-Th)/He dating: Techniques, calibrations, and applications. Reviews in Mineralogy and Geochemistry, 47(1): 819–844, doi: 10.2138/rmg.2002.47.18
Franke D, Savva D, Pubellier M, et al. 2014. The final rifting evolution in the South China Sea. Marine and Petroleum Geology, 58: 704–720, doi: 10.1016/j.marpetgeo.2013.11.020
Gallagher K, Brown R, Johnson C. 1998. Fission track analysis and its applications to geological problems. Annual Review of Earth and Planetary Sciences, 26: 519–572, doi: 10.1146/annurev.earth.26.1.519
Guenthner W R, Reiners P W, Ketcham R A, et al. 2013. Helium diffusion in natural zircon: Radiation damage, anisotropy, and the interpretation of zircon (U-Th)/He thermochronology. American Journal of Science, 313(3): 145–198, doi: 10.2475/03.2013.01
Hasebe N, Barbarand J, Jarvis K, et al. 2004. Apatite fission-track chronometry using laser ablation ICP-MS. Chemical Geology, 207(3–4): 135–145, doi: 10.1016/j.chemgeo.2004.01.007
Hu Anwen, Niu Chengmin, Wang Deying, et al. 2020. The characteristics and formation mechanism of condensate oil and gas in Bozhong19–6 structure, Bozhong sag, Bohai Bay Basin. Acta Petrolei Sinica (in Chinese), 41(4): 403–411
Ji Mo, Zeng Qingbo, Yang Haizhang, et al. 2021. Structural characteristics of central depression belt in deep-water area of the Qiongdongnan Basin and the hydrocarbon discovery of Songnan low bulge. Acta Oceanologica Sinica, 40(2): 42–53, doi: 10.1007/s13131-021-1753-y
Ketcham R A, Carter A, Donelick R A, et al. 2007. Improved measurement of fission-track annealing in apatite using c-axis projection. American Mineralogist, 92(5–6): 789–798, doi: 10.2138/am.2007.2280
Ketcham R A, Gautheron C, Tassan-Got L. 2011. Accounting for long alpha-particle stopping distances in (U–Th–Sm)/He geochronology: Refinement of the baseline case. Geochimica et Cosmochimica Acta, 75(24): 7779–7791, doi: 10.1016/j.gca.2011.10.011
Ketcham R A, Mora A, Parra M. 2018. Deciphering exhumation and burial history with multi-sample down-well thermochronometric inverse modelling. Basin Research, 30(S1): 48–64, doi: 10.1111/bre.12207
Lei Chao, Ren Jianye, Tong Dianjun. 2013. Geodynamics of the ocean-continent transition zone, northern margin of the South China Sea: implications for the opening of the South China Sea. Chinese Journal of Geophysics (in Chinese), 56(4): 1287–1299
Lei Jianshe, Zhao Dapeng, Steinberger B, et al. 2009. New seismic constraints on the upper mantle structure of the Hainan plume. Translated World Seismology, 173(1–2): 33–50
Li Chunfeng, Li Jiabiao, Ding Weiwei, et al. 2015. Seismic stratigraphy of the central South China Sea basin and implications for neotectonics. Journal of Geophysical Research: Solid Earth, 120(3): 1377–1399, doi: 10.1002/2014JB011686
Li Yamin, Shi Xiaobin, Xu Huilong, et al. 2012. Temporal and spatial distribution of tectonic subsidence and discussion on formation mechanism of anomalous post-rift tectonic subsidence in the Qiongdongnan basin. Journal of Jilin University (Earth Science Edition) (in Chinese), 42(1): 47–57,65
Li Chunfeng, Xu Xing, Lin Jian, et al. 2014. Ages and magnetic structures of the South China Sea constrained by deep tow magnetic surveys and IODP Expedition 349. Geochemistry, Geophysics, Geosystems, 15(12): 4958–4983
Li Youjuan, Zheng Dewen, Wu Ying, et al. 2017. A potential (U-Th)/He zircon reference material from Penglai zircon megacrysts. Geostandards & Geoanalytical Research, 41(3): 359–365
Lu Baoiang, Sun Xiaomeng, Zhang Gongcheng, et al. 2011. Seismic-potential field response characteristics and identification of basement lithology of the northern South China Sea basin. Chinese Journal of Geophysics (in Chinese), 54(2): 563–572
Ma Long, Liu Quanxin, Zhang Jinglian, et al. 2006. A discussion of exploration potentials of basement hydrocarbon reservoir. Natural Gas Industry (in Chinese), 26(1): 8–11
Maniar P D, Piccoli P M. 1989. Tectonic discrimination of granitoids. GSA Bulletin, 101(5): 635–643, doi: 10.1130/0016-7606(1989)101<0635:TDOG>2.3.CO;2
Mao Kainan, Xie Xinong, Xie Yuhong, et al. 2015. Post-rift tectonic reactivation and its effect on deep-water deposits in the Qiongdongnan Basin, northwestern South China Sea. Marine Geophysical Research, 36(2–3): 227–242, doi: 10.1007/s11001-015-9248-x
McKenzie D. 1978. Some remarks on the development of sedimentary basins. Earth and Planetary Science Letters, 40(1): 25–32, doi: 10.1016/0012-821X(78)90071-7
Mi Lijun, Tang Xiaoyin, Yang Haizhang, et al. 2023. Zircon U-Pb geochronology, Hf isotopes, and geochemistry constraints on the age and tectonic affinity of the basement granitoids from the Qiongdongnan Basin, northern South China Sea. Acta Oceanologica Sinica, 42(3): 19–30, doi: 10.1007/s13131-022-2078-1
Middlemost E A K. 1994. Naming materials in the magma/igneous rock system. Earth-Science Reviews, 37(3-4): 215–224, doi: 10.1016/0012-8252(94)90029-9
Morley C K, Westaway R. 2006. Subsidence in the super-deep Pattani and Malay basins of Southeast Asia: a coupled model incorporating lower-crustal flow in response to post-rift sediment loading. Basin Research, 18(1): 51–84, doi: 10.1111/j.1365-2117.2006.00285.x
Pan Jianguo, Hao Fang, Zhang Huquan, et al. 2007. Formation of granite and volcanic rock reservoirs and their accumulation model. Natural Gas Geoscience (in Chinese), 18(3): 380–385
Pang Jianzhang, Zheng Dewen, Ma Yan, et al. 2017. Combined apatite fission-track dating, chlorine and REE content analysis by LA-ICPMS. Science Bulletin, 62(22): 1497–1500, doi: 10.1016/j.scib.2017.10.009
Pearce J A, Harris N B W, Tindle A G. 1984. Trace element discrimination diagrams for the tectonic interpretation of granitic rocks. Journal of Petrology, 25(4): 956–983, doi: 10.1093/petrology/25.4.956
Qiu Nansheng, Wang Jiyang, Mei Qinghua, et al. 2010. Constraints of (U-Th)/He ages on early Paleozoic tectonothermal evolution of the Tarim Basin, China. Science China Earth Sciences, 53(7): 964–976, doi: 10.1007/s11430-010-4004-1
Qiu Nansheng, Zuo Yinhui, Chang Jian, et al. 2014. Geothermal evidence of Meso-Cenozoic lithosphere thinning in the Jiyang subbasin, Bohai Bay Basin, eastern North China Craton. Gondwana Research, 26(3–4): 1079–1092, doi: 10.1016/j.gr.2013.08.011
Ren Jinfeng, Cheng Cong, Xiong Pengfei, et al. 2022. Sand-rich gas hydrate and shallow gas systems in the Qiongdongnan Basin, northern South China Sea. Journal of Petroleum Science and Engineering, 215: 110630, doi: 10.1016/j.petrol.2022.110630
Ren Jianye, Zhang Daojun, Tong Dianjun, et al. 2014. Characterising the nature, evolution and origin of detachment fault in central depression belt, Qiongdongnan Basin of South China Sea: evidence from seismic reflection data. Acta Oceanologica Sinica, 33(12): 118–126, doi: 10.1007/s13131-014-0581-8
Rickwood P C. 1989. Boundary lines within petrologic diagrams which use oxides of major and minor elements. Lithos, 22(4): 247–263, doi: 10.1016/0024-4937(89)90028-5
Ru Ke, Pigott J D. 1986. Episodic rifting and subsidence in the South China Sea. AAPG Bulletin, 70(9): 1136–1155
Sajona F G, Maury R C, Bellon H, et al. 1993. Initiation of subduction and the generation of slab melts in western and eastern Mindanao, Philippines. Geology, 21(11): 1007–1010, doi: 10.1130/0091-7613(1993)021<1007:IOSATG>2.3.CO;2
Sehrt M, Glasmacher U A, Stockli D F, et al. 2017. Meso-/Cenozoic long-term landscape evolution at the southern Moroccan passive continental margin, Tarfaya Basin, recorded by low-temperature thermochronology. Tectonophysics, 717: 499–518, doi: 10.1016/j.tecto.2017.08.028
Shi Xiaobin, Jiang Haiyan, Yang Jun, et al. 2017. Models of the rapid post-rift subsidence in the eastern Qiongdongnan Basin, South China Sea: implications for the development of the deep thermal anomaly. Basin Research, 29(3): 340–362, doi: 10.1111/bre.12179

Shi Hesheng, Yang Jihai, Zhang Yingzhao, et al. 2019. Geological understanding innovation and major breakthrough to natural gas exploration in deep water in Qiongdongnan Basin. China Petroleum Exploration (in Chinese), 24(6): 691–698

Steckler M S, Watts A B. 1978. Subsidence of the Atlantic-type continental margin off New York. Earth and Planetary Science Letters, 41(1): 1–13, doi: 10.1016/0012-821X(78)90036-5

Stockli D F. 2005. Application of low-temperature thermochronometry to extensional tectonic settings. Reviews in Mineralogy and Geochemistry, 58(1): 411–448, doi: 10.2138/rmg.2005.58.16

Tang Xiaoyin, Zhang Gongcheng, Liang Jianshe, et al. 2013. Influence of igneous intrusions on the temperature field and organic maturity of the Changchang Sag, Qiongdongnan Basin, South China Sea. Chinese Journal of Geophysics (in Chinese), 56(1): 159–169

Tang Lishan, Zhu Jitian, Yao Zhe, et al. 2017. Evolution and reservoir formation conditions of buried hills in Songnan low uplift of the Qiongdongnan Basin. Special Oil and Gas Reservoirs (in Chinese), 24(1): 87–91

Tang Xiaoyin, Zuo Yinhui, Kohn B, et al. 2019. Cenozoic thermal history reconstruction of the Dongpu Sag, Bohai Bay Basin: insights from apatite fission-track thermochronology. Terra Nova, 31(3): 159–168, doi: 10.1111/ter.12379

Tu Jiyao, Ji Jianqing, Zhong Dalai, et al. 2021. The strong activities of the Namula fault zone in the eastern Himalayan syntaxis since the Pliocene, constraints from thermochronological data. Journal of Geomechanics (in Chinese), 27(4): 679–690

Vermeesch P. 2009. RadialPlotter: A Java application for fission track, luminescence and other radial plots. Radiation Measurements, 44(4): 409–410, doi: 10.1016/j.radmeas.2009.05.003

Wang Zhenfeng, Jiang Tao, Zhang Daojun, et al. 2015. Evolution of deepwater sedimentary environments and its implication for hydrocarbon exploration in Qiongdongnan Basin, northwestern South China Sea. Acta Oceanologica Sinica, 34(4): 1–10, doi: 10.1007/s13131-015-0645-4

Whalen J B, Currie K L, Chappell B W. 1987. A-type granites: Geochemical characteristics, discrimination and petrogenesis. Contributions to Mineralogy and Petrology, 95(4): 407–419, doi: 10.1007/BF00402202

Xie Xinong, Müller R D, Li Sitian, et al. 2006. Origin of anomalous subsidence along the Northern South China Sea margin and its relationship to dynamic topography. Marine and Petroleum Geology, 23(7): 745–765, doi: 10.1016/j.marpetgeo.2006.03.004

Xie Wenyan, Zhang Yiwei, Sun Zhen, et al. 2007. Characteristics and formation mechanism of faults in Qiongdongnan Basin. Marine Geology & Quaternary Geology (in Chinese), 27(1): 71–78

Xu Shouli, You Li, Mao Xuelian, et al. 2019b. Reservoir Characteristics and Controlling Factors of Granite Buried Hill in Songnan Low Uplift, Qiongdongnan Basin. Earth Science (in Chinese), 44(8): 2717–2728

Xu Changgui, Yu Haibo, Wang Jun, et al. 2019a. Formation conditions and accumulation characteristics of Bozhong 19–6 large condensate gas field in offshore Bohai Bay Basin. Petroleum Exploration and Development, 46(1): 27–40, doi: 10.1016/S1876-3804(19)30003-5

Yang Jun, Shi Xiaobin, Wang Zhenfeng, et al. 2015. Origin of syn-rift subsidence deficit and rapid post-rift subsidence in Qiongdongnan Basin. Marine Geology & Quaternary Geology (in Chinese), 35(1): 81–90

Yuan Yusong, Yang Shuchun, Hu Shengbiao, et al. 2008. Tectonic subsidence of Qiongdongnan Basin and its main control factors. Chinese Journal of Geophysics (in Chinese), 51(2): 376–383

Yuan Yusong, Zhu Weilin, Mi Lijun, et al. 2009. "Uniform geothermal gradient" and heat flow in the Qiongdongnan and Pearl River Mouth Basins of the South China Sea. Marine and Petroleum Geology, 26(7): 1152–1162, doi: 10.1016/j.marpetgeo.2008.08.008

Zhang Yingzhao, Gan Jun, Xu Xinde, et al. 2019. The source and natural gas lateral migration accumulation model of Y8–1 gas bearing structure, east deep water in the Qiongdongnan Basin. Earth Science (in Chinese), 44(8): 2609–2618

Zhao Zhongxian, Sun Zhen, Sun Longtao, et al. 2018. Cenozoic tectonic subsidence in the Qiongdongnan Basin, northern South China Sea. Basin Research, 30(S1): 269–288, doi: 10.1111/bre.12220

Zhao Zhongxian, Sun Zhen, Wang Zhenfeng, et al. 2013. The dynamic mechanism of post-rift accelerated subsidence in Qiongdongnan Basin, northern South China Sea. Marine Geophysical Research, 34(3–4): 295–308, doi: 10.1007/s11001-013-9188-2

Zhao Zhongxian, Sun Zhen, Wang Zhenfeng, et al. 2015. The high resolution sedimentary filling in Qiongdongnan Basin, Northern South China Sea. Marine Geology, 361: 11–24, doi: 10.1016/j.margeo.2015.01.002

Zhou Jie, Yang Xibing, Yang Jinhai, et al. 2019. Structure-sedimentary evolution and gas accumulation of Paleogene in Songnan low uplift of the Qiongdongnan Basin. Earth Science (in Chinese), 44(8): 2704–2716